Biomaterials Science

PAPER

View Article Online
View Journal | View Issue

Cite this: *Biomater. Sci.*, 2019, **7**, 4166

Azido-galactose outperforms azido-mannose for metabolic labeling and targeting of hepatocellular carcinoma†

Hua Wang, Yang Liu, Ming Xu and Jianjun Cheng *

Received 10th June 2019,
Accepted 4th July 2019

DOI: 10.1039/c9bm00898e

rsc.li/biomaterials-science

Metabolic glycoengineering of unnatural monosaccharides provides a facile method to label cancer cells with chemical tags for glycan imaging and cancer targeting. Multiple types of monosaccharides have been utilized for metabolic cell labeling. However, the comparison of different types of monosaccharides in labeling efficiency and selectivity has not been reported. In this study, we compared *N*-azidoacetylgalactosamine (GalAz) and *N*-azidoacetylmannosamine (ManAz) for metabolic labeling of HepG2 hepatocellular carcinoma *in vitro* and *in vivo*. GalAz showed higher labeling efficiency at low concentrations, and outperformed ManAz in metabolic labeling of HepG2 tumors *in vivo*. GalAz mediated labeling of HepG2 tumors with azido groups significantly improved the tumor accumulation of dibenzocyclooctyne (DBCO)–Cy5 and DBCO–doxorubicin conjugate *via* efficient Click chemistry. This study, for the first time, uncovered the distinct labeling efficiency and selectivity of different unnatural monosaccharides in liver cancers.

Introduction

Metabolic glycoengineering processing of unnatural sugars provides a powerful tool to label cell surface with chemical tags for glycan imaging and cell targeting.[1–4] These cell-surface chemical tags, coupled with efficient Click chemistries, have shown great potential for cancer targeting over the past few years due to the advantages in high targeting efficiency, absence of immunogenicity, and easy manufacturing.[5–9] In the first step, unnatural sugars carrying biorthogonal chemical groups (*e.g.*, azide) were delivered to and metabolized by cancers, followed by the targeting of dibenzocyclooctyne (DBCO)-bearing therapeutics *via* Click chemistry in the second step.[10] However, one challenge critical to the use of this two-step strategy for cancer targeting lies in cancer selective metabolic labeling.[11] Efforts have been made to deliver unnatural sugars in the form of nanoparticles by taking advantage of the enhanced permeability and retention (EPR) effect. For example, Kim *et al.* reported the use of chitosan nanoparticle for the delivery of tetraacetyl *N*-azidoacetylmannosamine (Ac_4ManAz).[12] Chen *et al.* reported the use of azido-sugar encapsulated liposomes for tumor labeling and subsequent targeting.[13,14] We recently reported the development of trigger-activatable Ac_3ManAz derivatives for cancer-selective labeling.[15,16] Other than these strategies, we envision that different types of unnatural sugars likely exhibit distinct metabolic labeling selectivity in varying types of cancers. Taking *N*-azidoacetylmannosamine (ManAz) and *N*-azidoacetylgalactosamine (GalAz) for example, they undergo different metabolic pathways, may have different tumor accumulation profiles, and exhibit different cancer-labeling kinetics.

Hepatocellular carcinoma (HCC) has become a leading cause of cancer patient deaths worldwide over the past decades.[17–19] Chemotherapy is a standard treatment for HCC in clinic, especially for advanced HCC.[20–22] For example, Sorafenib, a receptor tyrosine kinase inhibitor, has been approved by FDA to treat advanced HCC.[21] However, one key issue of chemotherapy is the severe side effect, and cancer-targeting strategy that can improve the tumor accumulation of chemotherapeutics while reducing their accumulation in healthy tissues is highly demanded.[21,23–25] Due to the absence of characteristic cell-surface receptors, targeted chemotherapy for HCC has been limited thus far. Asialoglycoprotein receptor (ASGPR) is one of few receptors overexpressed by HCC that could attach and clear glycoproteins with terminal galactose residues from the bloodstream.[26–28] Based on this, a variety of galactosylated nanoparticles have been developed for targeted delivery of therapeutics to liver cancers.[29–31] Given the higher affinity of galactoses over other monosaccharides to ASGPR,[32–34] we envision that GaAz might show higher tumor accumulation and metabolism rate in HCC in comparison to other azido-sugars including ManAz. In this study, we com-

Department of Materials Science and Engineering, University of Illinois at Urbana-Champaign, Urbana, Illinois 61801, USA. E-mail: jianjunc@illinois.edu

†Electronic supplementary information (ESI) available. See DOI: 10.1039/c9bm00898e

pared the HCC-labeling efficiency of GalAz and ManAz *in vitro* and *in vivo*, and evaluated the feasibility of applying GalAz and DBCO–drug conjugates to the targeted treatment of HCC.

Methods

Cell culture. HepG2 cancer cell was purchased from American Type Culture Collection (Manassas, VA, USA). Cells were cultured in DMEM containing 10% FBS, 100 units per mL Penicillin G and 100 μg mL^{-1} streptomycin (Invitrogen, Carlsbad, CA, USA) at 37 °C in 5% CO_2 humidified air unless otherwise noted.

Animals. Female athymic nude mice were purchased from Charles River (Wilmington, MA, USA). Feed and water were available *ad libitum*. Artificial light was provided in a 12 h/12 h cycle. The animal protocol was reviewed and approved by the Illinois Institutional Animal Care and Use Committee (IACUC) of University of Illinois at Urbana-Champaign. All animal procedures were performed in accordance with the Guidelines for Care and Use of Laboratory Animals of University of Illinois at Urbana-Champaign and approved by the Animal Ethics Committee of University of Illinois at Urbana-Champaign.

Synthesis of ManAz and GalAz. D-Mannosamine hydrochloride or D-galactosamine hydrochloride (1.0 mmol) and triethylamine (1.0 mmol) were dissolved in methanol, followed by the addition of *N*-(2-azidoacetyl) succinimide (1.1 mmol). The mixture was stirred at room temperature for 24 h. Solvent was removed under reduced pressure, and the crude product was purified by silica gel column chromatography using ethyl acetate to ethyl acetate/methanol (3/1, v/v) as the eluent to yield a light yellow solid. ESI MS (*m*/*z*): calculated for $C_8H_{14}N_4O_6Na$ $[M + Na]^+$ 285.1, found 285.1.

General procedures for confocal imaging of azido-sugar labeled cells. HepG2 cells were seeded onto coverslips in a 6-well plate at a density of 4×10^4 cells per well and allowed to attach for 12 h. GalAz or ManAz (200 μM) was added and the cells were incubated at 37 °C for 72 h. After washing with PBS, cells were incubated with DBCO–Cy5 (20 μM) for 40 min and fixed with 4% paraformaldehyde solution, followed by staining of cell nuclei with DAPI. The coverslips were mounted onto microscope slides and imaged under a confocal laser scanning microscope.

General procedures for flow cytometry analysis of azido-sugar labeled cells. HepG2 cells were seeded in a 24-well plate at a density of 1×10^4 cells per well and allowed to attach for 12 h. GalAz or ManAz (200 μM) was added and incubated with cells for 72 h. After washing with PBS, cells were incubated with DBCO–Cy5 (20 μM) for 40 min. Cells were lifted by incubating with trypsin solution and analyzed by flow cytometry.

Labeling kinetics of GalAz and ManAz. HepG2 cells were seeded in black 96-well plates and incubated with various concentrations of GalAz or ManAz (10 μM, 50 μM, 200 μM, 1 mM, and 5 mM) for different time (1, 6, 12, 24, 48, 72, 96, and 120 h). After washing with PBS, cells were incubated with DBCO–Cy5 (20 μM) for 40 min. Average Cy5 fluorescence intensity per cell was measured on IN Cell Analyzer 2200.

Synthesis of ^{14}C-Gal and ^{14}C-Man. 1-^{14}C acetic acid (1 molar equiv.) was dissolved in PBS (pH 7.4), followed by the addition of 1-ethyl-3-(3-dimethylaminopropyl)carbodiimide (EDC, 2 molar equiv.) and *N*-hydroxybenzotriazole (2 molar equiv.). The mixture was stirred at room temperature for 48 h. D-Mannosamine hydrochloride or D-galactosamine hydrochloride (1.0 molar equiv.) that had been neutralized by sodium bicarbonate was then added, and the mixture was further stirred at room temperature for 24 h. After filtration, the solution was concentrated for use.

^{14}C-Gal and ^{14}C-Man mediated cell labeling. HepG2 cells were seeded onto coverslips in a 6-well plate at a density of 4×10^4 cells per well and allowed to attach for 12 h. ^{14}C-Gal or ^{14}C-Man (1 μCi) was added and incubated with cells for 12 h. After washing with PBS, the cells were further incubated in fresh medium at 37 °C for 48 h. Cells were then harvested, lysed in the presence of EDTA-free protease inhibitor cocktail, and centrifuged to remove cell debris. The supernatant was collected for protein extraction following the reported procedures: nine volumes of ethanol were added to one volume of aqueous protein solution, and cooled at −80 °C for 4 h. The protein pellet was collected *via* centrifugation and re-dissolved in sodium dodecyl sulfate buffer upon heating. ^{14}C radioactivity of the extracted proteins was measured on a Tri-carb liquid scintillation counter. Ultima Gold™ liquid scintillation cocktail was used for the radioactivity measurement.

Biodistribution of ^{14}C-Gal and ^{14}C-Man. HepG2 tumors were established in 8 weeks-old female athymic nude mice by subcutaneous injection of HepG2 cells (1.5×10^6 cells) in Hank's balanced salt solution (HBSS)/matrigel (1/1, v/v) into both flanks. When the tumors reached ~70 mm^3, ^{14}C-Gal or ^{14}C-Man (10 μCi) was intravenously (i.v.) injected *via* tail vein. After 24 h or 5 days, tumors and organs were harvested, weighed, homogenized in lysis buffer, and measured for radioactivity on a Tri-Carb liquid scintillation counter. A gradient concentration of ^{14}C-Gal or ^{14}C-Man was used for determining the standard curve of ^{14}C radioactivity. The data were presented as the percentage of injected dose per gram tissue (% I.D. per g).

***In vivo* tumor labeling of GalAz and ManAz.** HepG2 tumors were established in 8 weeks-old female athymic nude mice by subcutaneous injection of HepG2 cells (1.5×10^6 cells) in HBSS/matrigel (1/1, v/v) into both flanks. When the tumors reached ~70 mm^3, mice were i.v. injected with GalAz or ManAz (200 mg kg^{-1}) once daily for three days (Day 1–3). Mice i.v. injected with PBS were used as controls. On Day 4, DBCO–Cy5 (5 mg kg^{-1}) was i.v. injected. Due to the intrinsic black color of HepG2 tumors, *in vivo* and *ex vivo* images of mice failed to show Cy5 fluorescence signals in tumors. At 48 h p.i. of DBCO–Cy5, tumors were harvested from mice and bisected. Half of the tumor was directly frozen in O.C.T. compound, sectioned with a thickness of 8 μm, stained with DAPI (2 μg mL^{-1}), and imaged under a confocal laser scanning microscope. Organs and the other half of tumors were homogenized and lysed. The lysates were measured on a fluorescence spectrometer to determine the amount of Cy5 retained in the tissues based on the standard curve of Cy5 fluorescence intensity. Data were presented as % I.D. per g.

Synthesis of pH-responsive DBCO-hz-Dox. DBCO-NHS (40.2 mg, 0.1 mmol) was dissolved in anhydrous acetonitrile (1 mL), followed by addition of hydrazine (16.0 mg, 0.5 mmol). The mixture was stirred at room temperature for 30 h. The solvent was removed and the residue redissolved in anhydrous DMF (500 μL). Doxorubicin hydrochloride (58.0 mg, 0.1 mmol) in DMF (500 μL) was added, followed by addition of one drop of concentrated hydrochloric acid. The reaction mixture was stirred at 40 °C for 48 h. DBCO-hz-Dox was obtained *via* precipitation of the reaction mixture into diethyl ether and washed with diethyl ether for twice (overall yield: 70%). LRMS (ESI) *m*/*z*: exact mass calculated for $C_{46}H_{45}N_4O_{12}$ $[M + H]^+$ 845.3, found 845.6.

Acute efficacy study. HepG2 tumor models were established in 6 weeks-old female 01B74 athymic nude mice by subcutaneous injection of HepG2 cells (1.5 million) into both flanks. When the tumors grew to a size of ~70 mm^3, GalAz or ManAz (200 mg kg^{-1}) was i.v. injected once daily for three days (Day 1–3). On Day 4, DBCO-hz-Dox (8 mg kg^{-1} Dox equivalent) was i.v. injected. At 48 h p.i. of DBCO-hz-Dox, tumors were

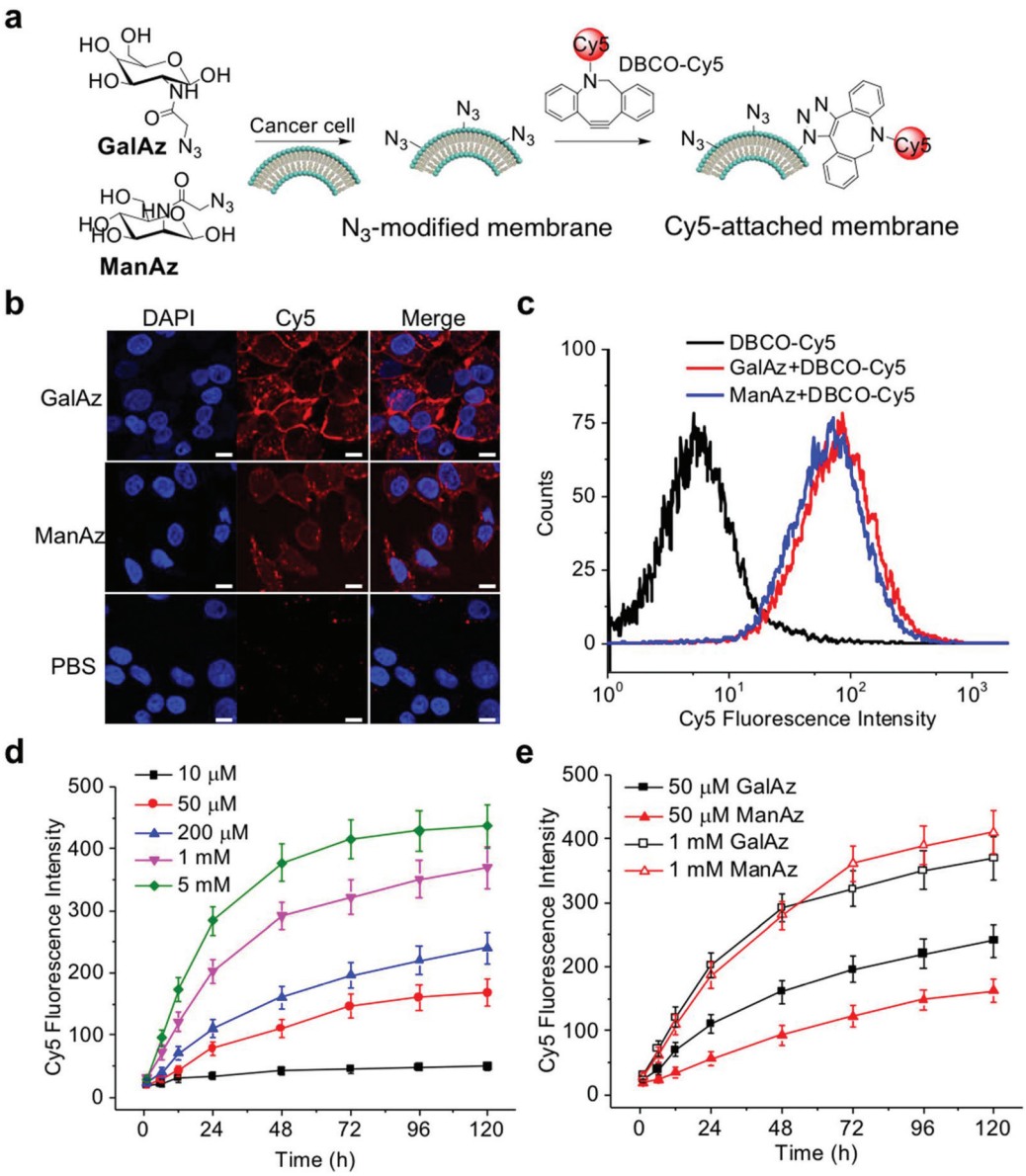

Fig. 1 (a) Schematic illustration of GalAz- or ManAz-mediated metabolic labeling of cancer cells with azido groups and subsequent detection by DBCO–Cy5 *via* Click chemistry. (b) CLSM images of HepG2 cells after treated with GalAz (200 μM), ManAz (200 μM), and PBS, respectively for 72 h and stained with DBCO–Cy5 (20 μM, red) for 40 min. Cell nuclei were stained with DAPI (blue). Scale bar: 10 μm. (c) Flow cytometry profiles of HepG2 cells following the same treatment in (b). (d) *In vitro* labeling kinetics of GalAz in HepG2 cells. HepG2 cells were incubated with different concentrations of GalAz (10 μM, 50 μM, 200 μM, 1 mM, and 5 mM) for different time (1, 6, 12, 24, 48, 72, 96, and 120 h), and stained with DBCO–Cy5 (20 μM) for 40 min. Average Cy5 fluorescence intensity was measured on a GE-analyzer. (e) Comparison of *in vitro* labeling kinetics of GalAz and ManAz at a concentration of 50 μM and 1 mM, respectively.

harvested from mice and bisected. Half of tumors were frozen with O.C.T. compound and sectioned on cryostat (Leica CM3050S) with a thickness of 6 μm. Cell apoptosis in tumors was analyzed *via* terminal deoxynucleotidyl transferase dUTP nick end labeling (TUNEL) assay using *in situ* cell death detection kit (Roche Diagnostics GmbH, Mannheim, Germany). The tumor sections were imaged with the confocal laser scanning microscopy (LSM 700, Zeiss). Cells under apoptosis were red fluorescent and all the nuclei were blue fluorescent. Organs and the other half of the tumors were homogenized and lysed in lysis buffer (1% SDS, 100 mM Tris·HCl, pH 7.4), treated with acids, and retained doxorubicin was quantified *via* HPLC.

Statistical analysis. Statistical analyses were conducted by Student's *t*-test (two-tailed) comparisons at 95% confidence interval. The results were deemed significant at $0.01 < {}^{*}P \leq 0.05$, highly significant at $0.001 < {}^{**}P \leq 0.01$, and extremely significant at ${}^{***}P \leq 0.001$.

Results and discussion

GalAz and ManAz were first synthesized and characterized *via* ^{1}H NMR, ^{13}C NMR and FTIR spectra (Scheme S1 and Fig. S1–3†). We first studied the metabolic labeling capability of GalAz and ManAz in HepG2 cancer cells *in vitro*. HepG2 cells were incubated with GalAz or ManAz for three days and the potentially expressed azido groups on the cell surface were detected by DBCO–Cy5 *via* Click chemistry (Fig. 1a). Cells pretreated with GalAz or ManAz showed much stronger Cy5 fluorescence intensity on the cell surface compared to control cells pretreated with PBS (Fig. 1b), indicating their successful expression of azido groups. It should be noted that the passive uptake of DBCO–Cy5 by HepG2 cells was negligible compared to covalently attached DBCO–Cy5 by cell-surface azido groups (Fig. 1b). Flow cytometry analysis of HepG2 cells also showed significantly enhanced Cy5 signal in cells pretreated with GalAz or ManAz (Fig. 1c). We next studied the *in vitro* labeling

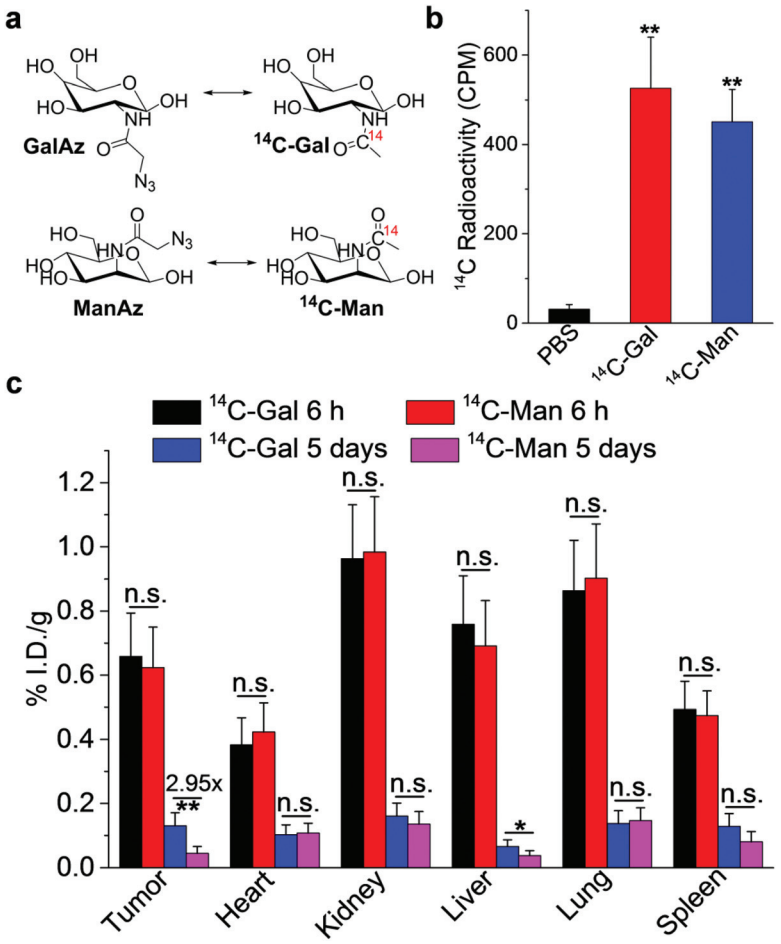

Fig. 2 (a) Structure of ^{14}C-Gal and ^{14}C-Man, as representatives of GalAz and ManAz, respectively. (b) ^{14}C radioactivity of proteins extracted from HepG2 cells after treatment with ^{14}C-Gal, ^{14}C-Man, and PBS, respectively. (c) Biodistribution of ^{14}C-Gal and ^{14}C-Man in athymic nude mice bearing subcutaneous HepG2 tumors at 6 h and 5 days p.i., respectively. Tissues were harvested from mice, homogenized, lysed, and measured for the radioactivity on a Tricarb liquid scintillation counter. All numerical data were presented as mean ± SD (n = 4) and analyzed by Student's *t*-test (two-tailed, $0.01 < {}^{*}P \leq 0.05$, $0.001 < {}^{**}P \leq 0.01$, and ${}^{***}P \leq 0.001$).

kinetics of GalAz and ManAz in HepG2 cells. HepG2 cells were incubated with different concentrations of GalAz or ManAz (10 μM, 50 μM, 200 μM, 1 mM, and 5 mM) for different time (1, 6, 12, 24, 48, 72, 96, and 120 h), and the expressed azido groups on the cell surface were detected by DBCO–Cy5. As a result, both GalAz- and ManAz-mediated labeling of HepG2 cancer cells was time- and concentration-dependent, with the azido expression approaching to a plateau value after 72 h (Fig. 1d and Fig. S4†). GalAz showed a faster metabolic labeling rate than ManAz at low concentrations (50 μM, Fig. 1e), but this difference became smaller at high sugar concentrations (1 mM, Fig. 1e), presumably because of saturated azido-expression. These experiments demonstrated that GalAz can metabolically label HepG2 cancer cells with azido groups and that GalAz exhibits a faster metabolic labeling rate than ManAz at low sugar concentrations.

We next aimed to compare the *in vivo* biodistribution profiles of GalAz and ManAz in mice bearing subcutaneous HepG2 tumors. However, it was unlikely to directly quantify GalAz and ManAz in tissues because of the change in chemical structure during sugar metabolism and lack of measurable properties. In addition, chemical modification of GalAz or ManAz with fluorescent or radioactive tags may significantly change their physiochemical and pharmacokinetic properties. Instead, we developed ^{14}C-Gal and ^{14}C-Man with a similar structure to GalAz and ManAz, respectively, to understand their biodistribution and tumor accumulation (Fig. 2a). We first studied whether ^{14}C-Gal and ^{14}C-Man could also metabolically label HepG2 cells *in vitro*. HepG2 cells were co-incubated with ^{14}C-Gal or ^{14}C-Man for 12 h and further incubated in fresh medium for 48 h. After washing, cells were lysed and proteins extracted for ^{14}C-radioactivity measurement. As a result, proteins extracted from cells treated with ^{14}C-Gal or ^{14}C-Man showed a significantly higher ^{14}C-radioactivity than control cells (Fig. 2b). These experiments suggested that ^{14}C-Gal and ^{14}C-Man can be metabolized by HepG2 cancer cells and be incorporated into cellular proteins.

After demonstrating the feasibility of using ^{14}C-Gal and ^{14}C-Man as representatives of GalAz and ManAz, we then studied the biodistribution of ^{14}C-Gal and ^{14}C-Man *in vivo*. HepG2 tumors were established in mice *via* subcutaneous injection of HepG2 cells into both flanks. When the tumors

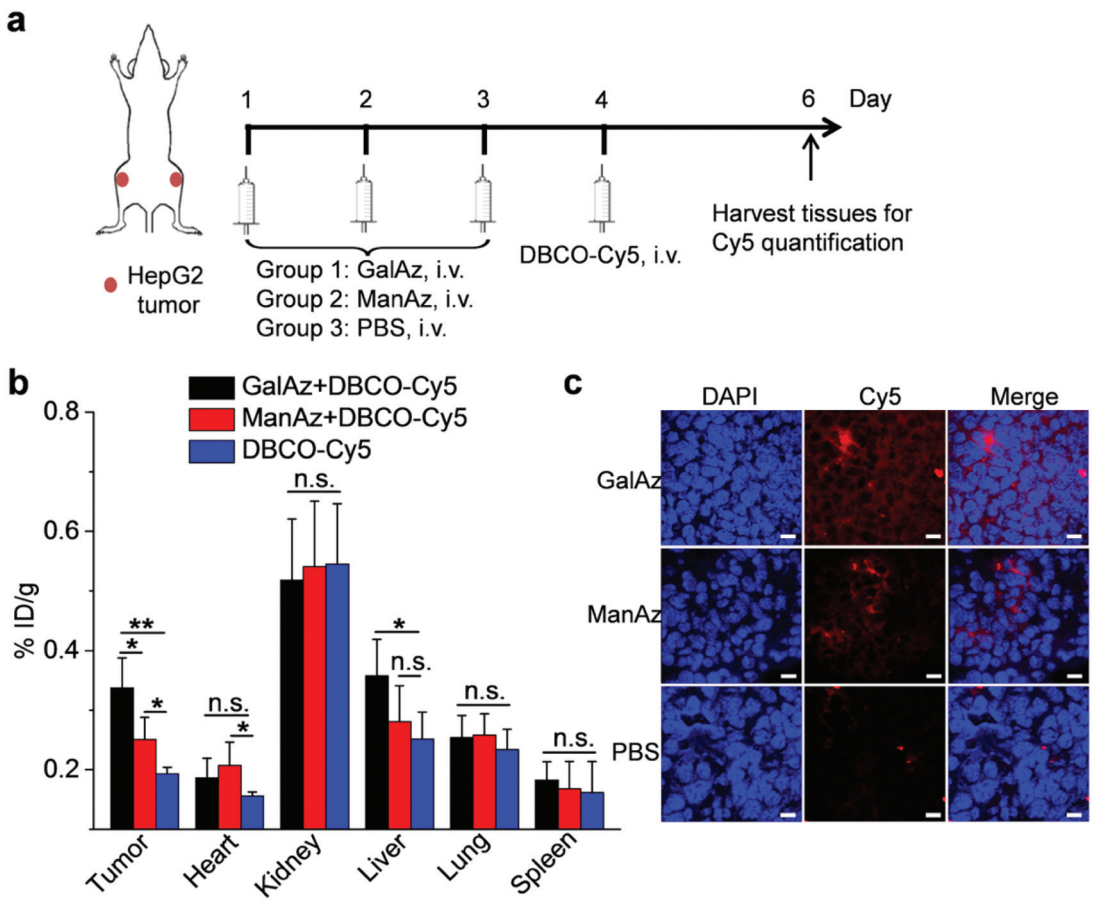

Fig. 3 (a) Time frame of *in vivo* metabolic labeling and targeting study. Athymic nude mice bearing subcutaneous HepG2 tumors were i.v. injected with GalAz (200 mg kg^{-1}), ManAz (200 mg kg^{-1}), and PBS, respectively once daily for three days. DBCO–Cy5 (5 mg kg^{-1}) was i.v. injected on Day 4. Tissues were harvested at 48 h p.i. of DBCO–Cy5 for Cy5 quantification. (b) Biodistribution of Cy5 in tissues at 48 h p.i. of DBCO–Cy5. Data were presented as mean ± SD (n = 4–5) and analyzed by Student's t-test (two-tailed, $0.01 < {}^{*}P \leq 0.05$, $0.001 < {}^{**}P \leq 0.01$, and ${}^{***}P \leq 0.001$). (c) Representative CLSM images of tumor tissue sections from different groups. Cell nuclei were stained with DAPI (blue). Scale bar: 10 μm.

grew to ~70 mm^3, mice were intravenously (i.v.) injected with ^{14}C-Gal or ^{14}C-Man. At 6 h or 5 days post injection (p.i.) of ^{14}C-Gal or ^{14}C-Man, tumors and organs were harvested, lysed, and measured for ^{14}C radioactivity. At 6 h p.i., ^{14}C-Gal and ^{14}C-Man showed similar accumulation in tissues including tumor, heart, kidney, liver, lung, and spleen (Fig. 2c). At 5 days p.i., ^{14}C-Gal showed much higher tumor retention than ^{14}C-Man, with a 195% enhancement (Fig. 2c). Compared to^{14}C-Man, ^{14}C-Gal also showed a higher retention in liver (Fig. 2c). The higher accumulation of ^{14}C-Gal in tumor and liver in comparison to ^{14}C-Man might be attributed to faster combined rate of cellular uptake and sugar metabolism. HepG2 tumor cells and hepatic cells are deemed rich in ASGPRs, and thus may preferentially bind ^{14}C-Gal. Since the concentration of intratumoral ^{14}C-Gal and ^{14}C-Man is relatively low, ^{14}C-Gal may show a faster metabolic labeling rate than ^{14}C-Man (Fig. 1e). ^{14}C-Gal showed better long-term retention in tumors than in livers (Fig. 2c), presumably because of the higher sugar metabolism rate in cancer cells than in normal cells.[15] These experiments indicate the better long-term tumor retention and metabolic labeling of GalAz than ManAz in HepG2 tumors.

We next studied whether i.v. injected GalAz and ManAz could efficiently label HepG2 tumors with azido groups *in vivo* and subsequently mediate targeted delivery of DBCO–Cy5. HepG2 tumors were established in athymic nude mice by subcutaneous injection of HepG2 cancer cells into both flanks. When the tumors reached ~70 mm^3, GalAz or ManAz was i.v. injected once daily for three days (Day 1–3). DBCO–Cy5 was i.v. injected on Day 4 (Fig. 3a). Because of the black color of HepG2 tumors, *in vivo* whole-body imaging and *ex vivo* imaging of harvested tissues failed to provide useful information about Cy5 accumulation in tissues. We homogenized the tissues at 48 h p.i. of DBCO–Cy5, and quantified the retained Cy5. Mice treated with GalAz or ManAz showed significantly improved tumor accumulation of DBCO–Cy5 than mice treated with PBS (Fig. 3b), indicating the covalent capture of DBCO–Cy5 by azido-labeled tumor cells *via* Click chemistry. The accumulation of DBCO–Cy5 in livers was also enhanced in

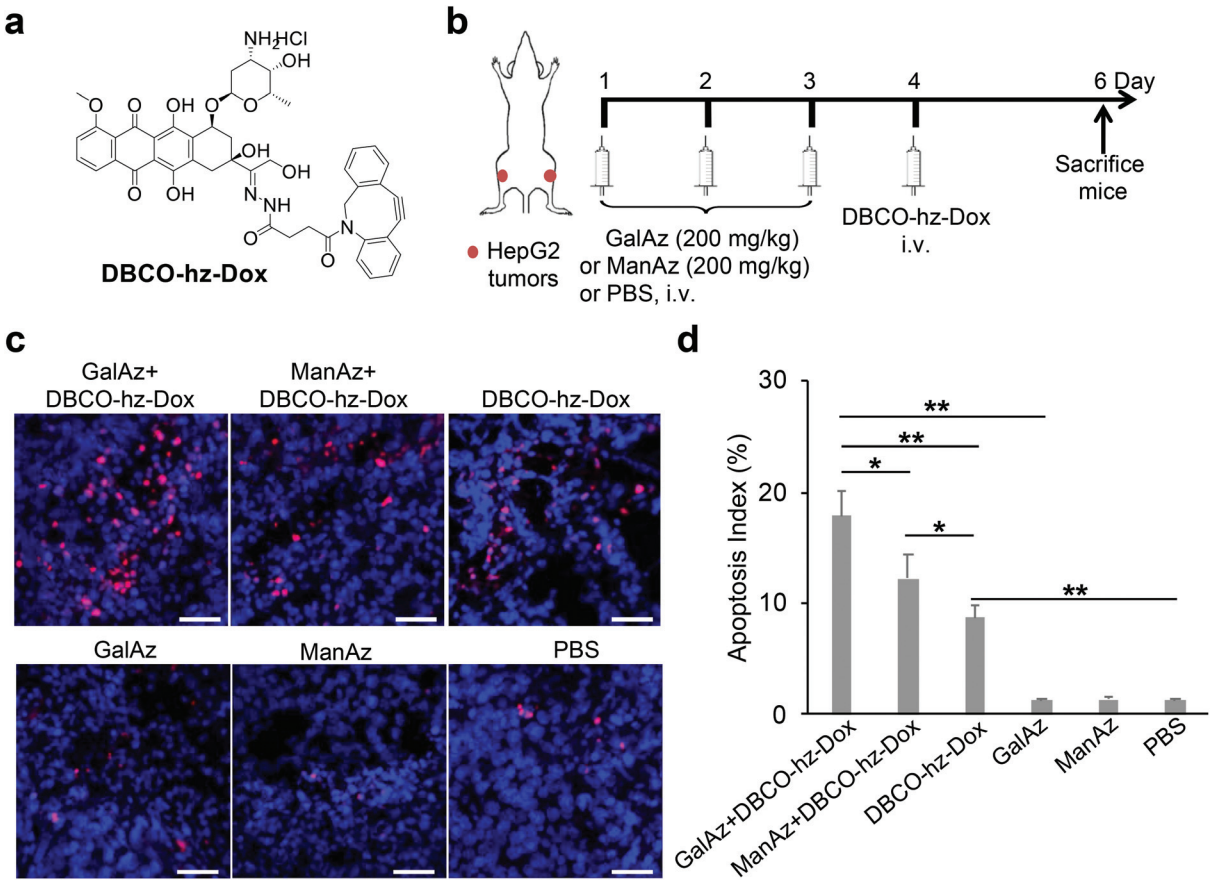

Fig. 4 (a) Structure of pH-responsive DBCO–doxorubicin conjugate, DBCO-hz-Dox. (b) Time frame of acute efficacy study. Athymic nude mice bearing HepG2 tumors were i.v. injected with Gal-N_3 (200 mg kg^{-1}) or Man-N_3 (200 mg kg^{-1}) or PBS once daily for three days. DBCO-hz-Dox (8.0 mg kg^{-1}, Dox equivalent) was i.v. injected on Day 4. Tissues were harvested from mice at 48 h p.i. of DBCO-hz-Dox. (c) Representative TUNEL staining sections of HepG2 tumors from mice treated with GalAz + DBCO-hz-Dox, ManAz + DBCO-hz-Dox, DBCO-hz-Dox, GalAz, ManAz, and PBS, respectively. Scale bar: 50 μm. (d) Quantification of TUNEL stains *via* ImageJ. The apoptosis index was determined as the ratio of apoptotic cell number (TUNEL, red) to the total cell number (DAPI, blue). 20 tissue sections were counted per tumor; $n = 5$. Statistical significance analysis was performed by Student's *t*-test (two tailed, $0.01 < {*}P \leq 0.05$, $0.001 < {**}P \leq 0.01$, and ${***}P \leq 0.001$).

GalAz- or ManAz-treated mice compared to PBS-treated mice, but to a less extent (Fig. 3b). Compared to ManAz, GalAz treatment significantly improved the tumor accumulation of DBCO–Cy5 (Fig. 3b), presumably due to the expression of a higher amount of azido groups. Confocal images of tumor tissues also showed stronger Cy5 fluorescence intensity in GalAz group in comparison to ManAz group (Fig. 3c). These experiments demonstrate that GalAz outperformed ManAz for *in vivo* metabolic labeling of HepG2 tumors with azido groups and subsequent targeting of DBCO-cargo.

After demonstrating that GalAz- and ManAz-mediated labeling of HepG2 tumors could enhance tumor accumulation of DBCO–Cy5 *via* Click chemistry, we next investigated whether GalAz or ManAz pretreatment would improve tumor accumulation of DBCO–drug conjugate. DBCO–doxorubicin conjugate with a pH-responsive hydrazone linker, DBCO-hz-Dox, was synthesized (Fig. 4a). DBCO-hz-Dox showed great stability under physiological conditions (pH 7.4), but underwent rapid degradation and Dox release at pH 5.0 (Fig. S5†). In an acute antitumor efficacy study, when subcutaneous HepG2 tumors reached ~70 mm^3, mice were i.v. injected with GalAz or ManAz once daily for three days. DBCO-hz-Dox was i.v. injected on Day 4. At 48 h p.i. of DBCO-hz-Dox, tumor tissues were harvested for the analyses of drug retention and tumor cell apoptosis (Fig. 4b). As a result, mice treated with GalAz showed significantly enhanced tumor accumulation of DBCO-hz-Dox than mice treated with ManAz or PBS (Fig. S6†). All drug treatment groups showed much higher tumor apoptosis than GalAz alone, ManAz alone, and PBS groups (Fig. 4c and d). Compared to DBCO-hz-Dox only (8.7%), GalAz + DBCO-hz-Dox (17.9%) and ManAz + DBCO-hz-Dox (12.2%) resulted in greater tumor apoptosis (Fig. 4c and d). In comparison to ManAz, GalAz treatment further improved the tumor accumulation of DBCO-hz-Dox (Fig. S6†) and the resulting tumor apoptosis (Fig. 4c and d). These experiments demonstrate that GalAz-mediated metabolic labeling of HepG2 tumors can improve the tumor accumulation of DBCO–drug conjugate and impart higher antitumor efficacy.

Conclusion

To conclude, we showed that GalAz can metabolically label HepG2 tumors *in vitro* and *in vivo*, and demonstrated the feasibility of coupling GalAz labeling with DBCO–drug conjugates for targeted treatment of liver cancers. Compared to ManAz, GalAz showed a slightly faster cell-labeling rate at low sugar concentrations *in vitro*, and a significantly higher long-term tumor retention and metabolic labeling efficiency *in vivo*. GalAz-mediated labeling of HepG2 tumors could significantly improve the tumor accumulation of DBCO–Cy5 and DBCO–doxorubicin conjugate *via* Click chemistry, and resulted in improved anticancer efficacy in an acute efficacy study. The combination of GalAz and DBCO–drug conjugates will provide a new avenue for targeted treatment of HCC. This study, for the first time, demonstrates the distinct tumor labeling efficiency of unnatural sugars derived from different monosaccharides in liver cancers. It is possible that unnatural sugars, without any further chemical modification, could have intrinsical labeling selectivity for certain types of cancers.

Conflicts of interest

The authors declare no competing financial interest.

Acknowledgements

J. C. acknowledges financial supports from NIH (R01 EB025651). H. W. is funded by Howard Hughes Medical Institute International Student Research Fellowship.

References

1 P. V. Chang, X. Chen, C. Smyrniotis, A. Xenakis, T. Hu, C. R. Bertozzi and P. Wu, *Angew. Chem., Int. Ed.*, 2009, **48**, 4030–4033.
2 H. C. Hang, C. Yu, D. L. Kato and C. R. Bertozzi, *Proc. Natl. Acad. Sci. U. S. A.*, 2003, **100**, 14846–14851.
3 T.-L. Hsu, S. R. Hanson, K. Kishikawa, S.-K. Wang, M. Sawa and C.-H. Wong, *Proc. Natl. Acad. Sci. U. S. A.*, 2007, **104**, 2614–2619.
4 S. T. Laughlin, N. J. Agard, J. M. Baskin, I. S. Carrico, P. V. Chang, A. S. Ganguli, M. J. Hangauer, A. Lo, J. A. Prescher and C. R. Bertozzi, *Methods Enzymol.*, 2006, **415**, 230–250.
5 J. E. Moses and A. D. Moorhouse, *Chem. Soc. Rev.*, 2007, **36**, 1249–1262.
6 J. M. Baskin, J. A. Prescher, S. T. Laughlin, N. J. Agard, P. V. Chang, I. A. Miller, A. Lo, J. A. Codelli and C. R. Bertozzi, *Proc. Natl. Acad. Sci. U. S. A.*, 2007, **104**, 16793–16797.
7 M. M. Kamphuis, A. P. Johnston, G. K. Such, H. H. Dam, R. A. Evans, A. M. Scott, E. C. Nice, J. K. Heath and F. Caruso, *J. Am. Chem. Soc.*, 2010, **132**, 15881–15883.
8 H. Koo, S. Lee, J. H. Na, S. H. Kim, S. K. Hahn, K. Choi, I. C. Kwon, S. Y. Jeong and K. Kim, *Angew. Chem., Int. Ed.*, 2012, **51**, 11836–11840.
9 R. Rossin, P. Renart Verkerk, S. M. van den Bosch, R. Vulders, I. Verel, J. Lub and M. S. Robillard, *Angew. Chem., Int. Ed.*, 2010, **49**, 3375–3378.
10 H. Wang, L. Tang, Y. Liu, I. T. Dobrucka, L. W. Dobrucki, L. Yin and J. Cheng, *Theranostics*, 2016, **6**, 1467–1476.
11 P. V. Chang, D. H. Dube, E. M. Sletten and C. R. Bertozzi, *J. Am. Chem. Soc.*, 2010, **132**, 9516–9518.
12 S. Lee, H. Koo, J. H. Na, S. J. Han, H. S. Min, S. J. Lee, S. H. Kim, S. H. Yun, S. Y. Jeong, I. C. Kwon, K. Choi and K. Kim, *ACS Nano*, 2014, **8**, 2048–2063.
13 R. Xie, L. Dong, R. Huang, S. Hong, R. Lei and X. Chen, *Angew. Chem., Int. Ed.*, 2014, **53**, 14082–14086.

14 R. Xie, S. Hong, L. Feng, J. Rong and X. Chen, *J. Am. Chem. Soc.*, 2012, **134**, 9914–9917.
15 H. Wang, R. Wang, K. Cai, H. He, Y. Liu, J. Yen, Z. Wang, M. Xu, Y. Sun, X. Zhou, Q. Yin, L. Tang, I. T. Dobrucki, L. W. Dobrucki, E. J. Chaney, S. A. Boppart, T. M. Fan, S. Lezmi, X. Chen, L. Yin and J. Cheng, *Nat. Chem. Biol.*, 2017, **13**, 415.
16 R. Wang, K. Cai, H. Wang, C. Yin and J. Cheng, *Chem. Commun.*, 2018, **54**, 4878–4881.
17 J. Bruix and M. Sherman, *Hepatology*, 2011, **53**, 1020–1022.
18 H. B. El-Serag and A. C. Mason, *N. Engl. J. Med.*, 1999, **340**, 745–750.
19 S. F. Altekruse, K. A. McGlynn and M. E. Reichman, *J. Clin. Oncol.*, 2009, **27**, 1485–1491.
20 J. M. Llovet and J. Bruix, *Hepatology*, 2003, **37**, 429–442.
21 J. M. Llovet, S. Ricci, V. Mazzaferro, P. Hilgard, E. Gane, J.-F. Blanc, A. C. de Oliveira, A. Santoro, J.-L. Raoul and A. Forner, *N. Engl. J. Med.*, 2008, **359**, 378–390.
22 M. B. Thomas, J. P. O'Beirne, J. Furuse, A. T. Chan, G. Abou-Alfa and P. Johnson, *Ann. Surg. Oncol.*, 2008, **15**, 1008–1014.
23 J. M. Llovet and J. Bruix, *Hepatology*, 2008, **48**, 1312–1327.
24 A. Villanueva and J. M. Llovet, *Gastroenterology*, 2011, **140**, 1410–1426.
25 S. Tanaka and S. Arii, *Cancer Sci.*, 2009, **100**, 1–8.
26 C. Plank, K. Zatloukal, M. Cotten, K. Mechtler and E. Wagner, *Bioconjugate Chem.*, 1992, **3**, 533–539.
27 R. J. Stockert, *Physiol. Rev.*, 1995, **75**, 591–609.
28 Y. Li, G. Huang, J. Diakur and L. I. Wiebe, *Curr. Drug Delivery*, 2008, **5**, 299–302.
29 S. Pranatharthiharan, M. D. Patel, V. C. Malshe, V. Pujari, A. Gorakshakar, M. Madkaikar, K. Ghosh and P. V. Devarajan, *Drug Delivery*, 2017, **24**, 20–29.
30 F. Kratz, *J. Controlled Release*, 2008, **132**, 171–183.
31 Z. Xu, L. Chen, W. Gu, Y. Gao, L. Lin, Z. Zhang, Y. Xi and Y. Li, *Biomaterials*, 2009, **30**, 226–232.
32 A. A. D'Souza and P. V. Devarajan, *J. Controlled Release*, 2015, **203**, 126–139.
33 D. Stokmaier, O. Khorev, B. Cutting, R. Born, D. Ricklin, T. O. Ernst, F. Böni, K. Schwingruber, M. Gentner and M. Wittwer, *Bioorg. Med. Chem.*, 2009, **17**, 7254–7264.
34 H.-X. Wang, M.-H. Xiong, Y.-C. Wang, J. Zhu and J. Wang, *J. Controlled Release*, 2013, **166**, 106–114.